

Diffusion and Kirkendall effect in PbSe–EuS multilayer

A. Fedorov^{a,*}, A. Sipatov^b, V. Volobuev^b

^a*Institute for Single Crystals, Kharkov 61001, Ukraine*

^b*National Technical University 'KPI', Kharkov 61002, Ukraine*

Received 31 July 2002; received in revised form 16 October 2002; accepted 15 November 2002

Abstract

Epitaxial PbSe–EuS multilayer subjected to diffusion annealing was examined by low-angle X-ray diffraction and Bragg X-ray diffraction. Multilayer profile change in the course of diffusion intermixing was determined by simulation of X-ray diffraction on the model multilayer profile and comparison of calculated patterns with experimental ones. The systematic shift of the average Bragg peak found at diffusion shows the presence of Kirkendall effect in the specimen. Matano procedure was applied to calculate the partial diffusion coefficients of the multilayer components.

© 2002 Elsevier Science B.V. All rights reserved.

Keywords: Annealing; Multilayers; Diffusion; X-ray diffraction

1. Introduction

Semiconductor superlattices of A^4B^6 compounds are preferable objects for investigation of phenomena in low dimensional structures, among them resonant tunneling [1], thermoelectric effect with increased figure of merit [2], ferromagnetic ordering [3], etc. These compounds have a simple crystalline structure (NaCl type) with lattice periods close to each other and allow to prepare single crystalline epitaxial films on different substrates (KCl, BaF₂, Si), usable to produce multilayers consisting of narrow-gap (PbS, PbSe, PbTe, SnTe) and wide-gap (EuS, EuSe, EuTe, YbS, YbSe, YbTe) semiconductor layers with layer thicknesses down to 1 nm.

Abrupt transitions between layers, flat interfaces and stability under external thermal or radiation influence are important features for manifestation of the above-mentioned phenomena. In this work the evolution of PbSe–EuS multilayer profile under thermal annealing was examined.

2. Specimens and methods

Epitaxial multilayers were grown in a high vacuum oil-free chamber on (1 0 0) oriented KCl cleavage plane

*Corresponding author. Tel.: +380-572-30-79-58; fax: +380-572-32-02-73.

E-mail address: fedorov@xray.isc.kharkov.com (A. Fedorov).

with preliminary grown PbS buffer layer. Used A^4B^6 compounds were *n*-PbSe and *n*-PbS 99.995% (metal basis) from Alfa Aesar Johnson Matthey GmbH (www.alfa-chemcat.com) and EuS 99.98% (metal basis) synthesized in the Institute of Solid State Physics, Chernogolovka, Russia (for more information about quality of EuS material see Ref. [11]).

Thin films of EuS and PbSe were deposited alternatively by electron beam and thermal evaporation of initial compounds. Film thicknesses and multilayer period uniformity were controlled with quartz oscillator mounted near the substrate. Finally, the multilayer was covered with protecting EuS cap. During deposition, vacuum was maintained at 1.33×10^{-6} Pa level. The ready specimen consists of 20 alternating films (10 periods) of EuS and PbSe with additional 50 nm thick PbS buffer and EuS cap, the multilayer period being 10.7 nm. To avoid the superposition of strong KCl (2 0 0) reflection on the multilayer diffraction curve at subsequent X-ray investigations, the multilayer was got free by dissolving KCl substrate in distilled water and drawn out to a glass substrate. The specimen annealing was performed in vacuum chamber at 660 K. Total annealing duration was 59 h. In the course of annealing, the specimen was periodically taken out of the chamber for X-ray diffraction investigation.

The multilayer structure was examined using low-angle X-ray diffraction of Cu $K\alpha$ radiation and Bragg X-ray diffraction at (2 0 0) reflection. These two methods are often used simultaneously [4,5] allowing to obtain more comprehensive information on multilayer structure. The reason is that the Bragg diffraction pattern of multilayer is formed both by interplanar distance distribution and electron density distribution across the multilayer, while the low angle diffraction is dependent only on the dielectric constant profile of multilayer.

3. Results

A typical shape of the Bragg diffraction pattern obtained from the single crystalline multilayer consists of the central peak in which the position is defined by the average lattice parameter and a set of satellites on both sides of the average peak. The distances between peaks, their relative intensities and position of the whole pattern are dependent on the multilayer composition, period, and cross-section profile. The diffraction pattern shape may be simulated by calculating the X-ray diffraction for a model multilayer profile. In this work, this was done by numerical solving of Takagi–Taupin equations [6] for diffraction on the model profile and then varying the model parameters to achieve the best fit between the experimental and calculated diffraction patterns. The results of fitting for some annealing stages are shown in Fig. 1.

The interdiffusion through the layer boundaries on annealing leads to the multilayer profile smoothing. The model multilayer profile was constructed from solution of the diffusion equation

$$F(z,t) = \sum_n a_n \cos\left(\frac{2\pi n}{H} z\right) \exp\left(-\frac{4\pi^2 n^2 D t}{H^2}\right) \quad (1)$$

Here H is the multilayer period; D , diffusion coefficient; t , annealing time.

It is evident that in the initial moment, $F(z,0)$ represents the Fourier expansion of initial rectangular profile

$$F(z,0) = \sum_n a_n \cos\left(\frac{2\pi n}{H} z\right), \quad a_0 = S, \quad (2)$$

$$a_n = \frac{2}{n\pi} \sin(n\pi S)$$

where S is the symmetry factor of multilayer introduced as $S = h_{\text{PbTe}}/H$.

The profile smoothing due to diffusion is defined by dependence of the expansion coefficients on Dt

$$a_n(t) = a_n(0) \exp(-4\pi^2 n^2 D t / H^2) \quad (3)$$

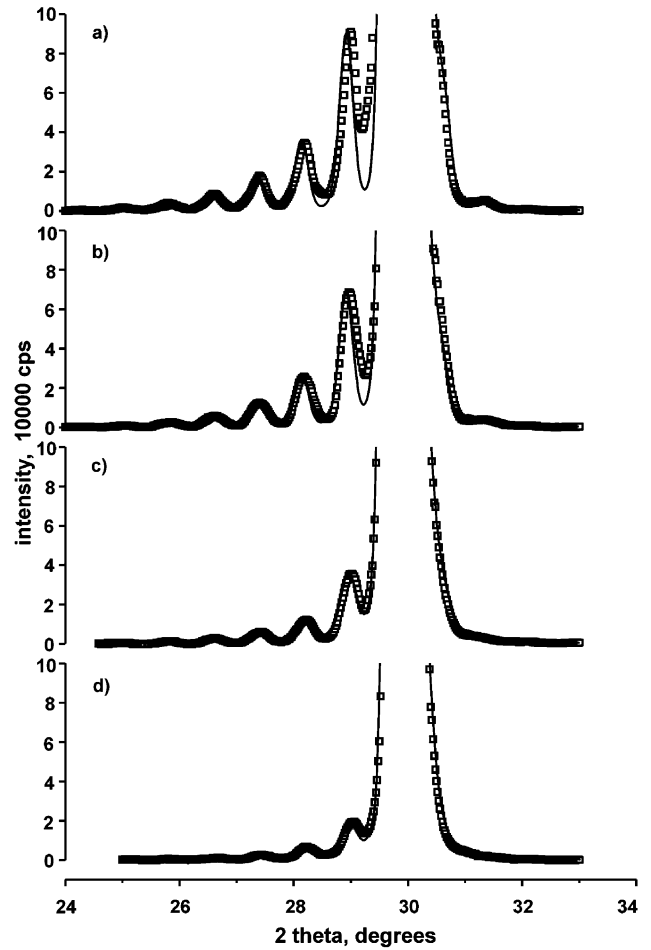


Fig. 1. Normalized experimental (dots) and calculated (line) Bragg diffraction patterns in the course of diffusion: initial state (a) and after 2 h (b); 20 h (c); 50 h (d) of annealing.

Such defined modulating function $F(z,t)$ was applied to obtain the periodical variation of interplanar distance in the normal direction z to the surface and modulation of polarizability that are members of Takagi–Taupin equation

$$\frac{dY}{dz} = i \frac{\pi}{L_e} [Y^2 - 2(\eta - f)Y + 1] \quad (4)$$

Here, Y is the ratio of diffracted to initial beam amplitudes; L_e , the extinction distance; η , the normalized angular variable; f , the normalized variation of interplanar distance along z . The value f is introduced as $f = 2\varepsilon(z,t) \sin^2 \vartheta / \chi_{\text{hr}}$, $\varepsilon(z,t) = F(z,t)(d_{\text{PbTe}} - d_{\text{EuS}}) / d_{\text{avg}}$. Modulation of polarizability χ_{hr} was defined in the same manner.

Interpretation of low-angle diffraction patterns is based on the Fresnel equations [7,8]. At a grazing incident beam, the diffraction is insensitive to the interplanar distance distribution on the atomic scale, but is the result of X-rays interference scattered at the layer

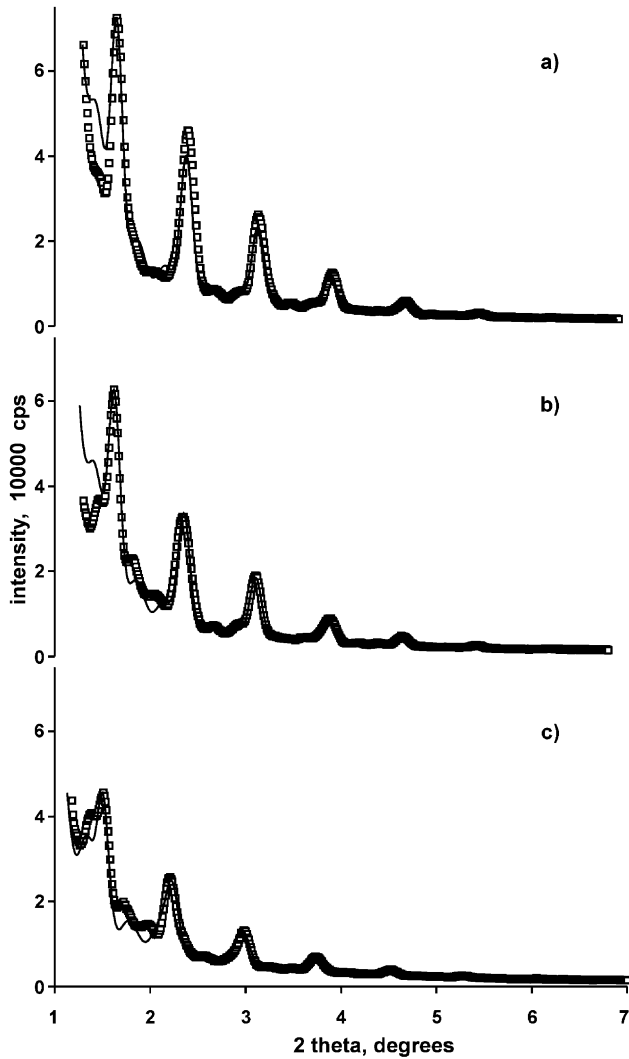


Fig. 2. Experimental (dots) and calculated (line) low angle diffraction patterns during annealing: initial state (a); after 3 h (b) and after 20 h (c) of annealing. Additional intensities between the main peaks are connected with the presence of the EuS cap.

interfaces due to the difference in dielectric constant. Simulation of multilayer reflectivity R in the low angle range was executed with the following set of recurrent equations

$$\begin{aligned}
 R_j &= \frac{R_j^F + R_{j+1} \exp 2i\chi_{j+1} h_{j+1}}{1 + R_j^F R_{j+1} \exp 2i\chi_{j+1} h_{j+1}} \\
 R_M &= R_M^F \\
 R_j^F &= \frac{\sqrt{\epsilon_j - \sin^2 \varphi_0} - \sqrt{\epsilon_{j+1} - \sin^2 \varphi_0}}{\sqrt{\epsilon_j - \sin^2 \varphi_0} + \sqrt{\epsilon_{j+1} - \sin^2 \varphi_0}} \\
 \chi_{j+1} &= \frac{2\pi}{\lambda} \sqrt{\epsilon_{j+1} - \sin^2 \varphi_0}
 \end{aligned} \tag{5}$$

Here, R_j is the reflection at the j th interface counted from the surface; R_M , reflection at the boundary with substrate that comes as the initial condition; ϵ_j , complex

dielectric constant of j th layer; φ_0 , angle between the normal to multilayer surface and incident beam. The experimental low angle patterns and fitted ones are shown in Fig. 2. Evolution of the dielectric constant profile in the course of diffusion was modelled using Eqs. (1)–(3).

In the process of diffusion in multilayer and simulation of successive diffraction patterns the regular shift of the average lattice peak position was revealed (Fig. 3). This means that the relation of layers thicknesses, or the multilayer symmetry factor, is changed due to diffusion intermixing. The change of symmetry factor is expressed as $S = 1 - (d_{\text{PbTe}} - d_{\text{avg}}) / (d_{\text{PbTe}} - d_{\text{EuS}})$, where d_{avg} corresponds to the interplanar distance derived from the position of the average peak. This phenomena may be interpreted as the occurrence of Kirkendall effect in the thin film multilayer. Behaviour character of the Bragg diffraction pattern depending separately on the diffusion length \sqrt{Dt} and on the change of the multilayer symmetry factor is essentially different. So the simulation of the Bragg diffraction patterns was performed considering both factors, using the data shown in Fig. 3. This allowed to calculate the multilayer profile in the course of diffusion as a result of fitting of the diffraction patterns (Fig. 4).

The multilayer diffusion parameters were calculated using the Boltzmann–Matano analysis [9]. The position of Matano plane was defined from

$$\int_{z_M}^{H/2} C(z,t) dz = \int_0^{z_M} [1 - C(z,t)] dz \tag{6}$$

where $C(z,t)$ is the molar concentration of component (Fig. 5). The concentration profiles were taken in from Eqs. (1)–(3). Applying it to Eq. (6) yields

$$\frac{z_M}{H} = \frac{S}{2} + \frac{1}{\pi^2} \sum_{n=1}^N \frac{\sin n \pi S}{n^2} \exp\left(-\frac{4\pi^2 n^2 Dt}{H^2}\right) \sin n \pi \tag{7}$$

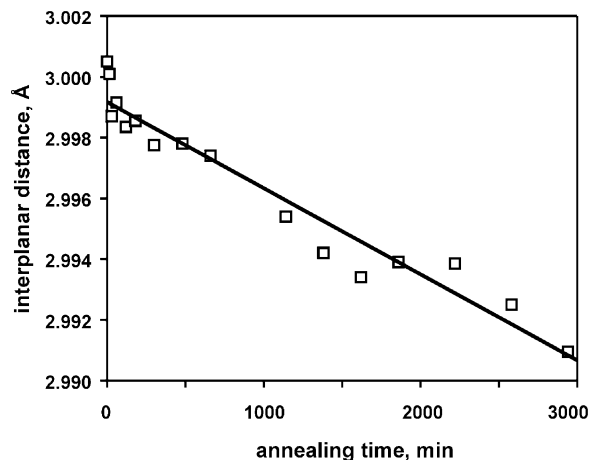


Fig. 3. Average Bragg peak shift in the course of diffusion. Interplanar distance change of the average lattice is shown.

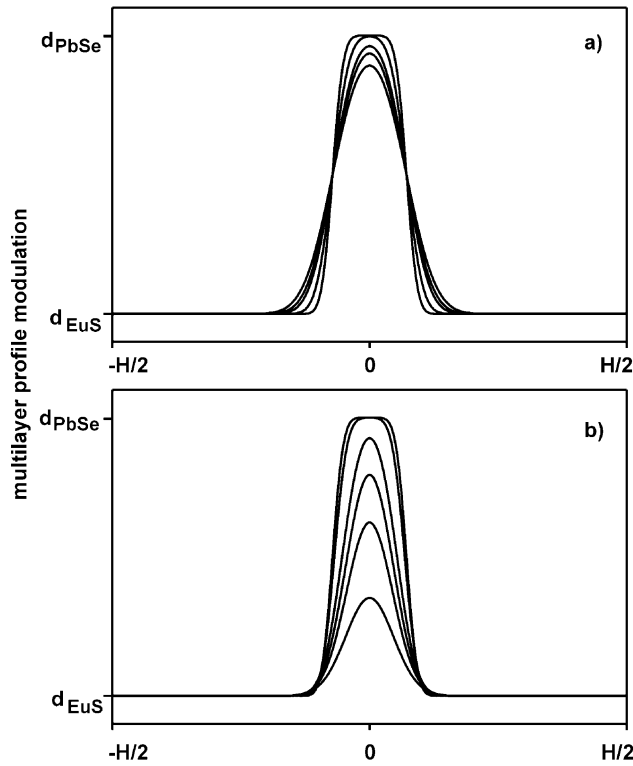


Fig. 4. Change of calculated multilayer profiles (single period) according to Eqs. (1)–(3) in the course of diffusion intermixing. The set (a) of profiles calculated at constant $S=0.144$ and consequence of diffusion lengths 1.24, 1.87, 2.63, 2.95 and 3.39 Å, while the set (b) is derived from measured symmetry factor change and fitting of experimental diffraction patterns. Modulation of interplanar distance is shown.

The area under concentration profile limited by z_M is

$$Q = S \left(\frac{H}{2} - z_M \right) + \frac{H}{\pi^2} \sum_{n=1}^N \frac{\sin n \pi S}{n^2} \exp \left(- \frac{4 \pi^2 n^2 D t}{H^2} \right) \times \left(\sin n \pi - \sin \frac{2 n \pi z_M}{H} \right) \quad (8)$$

The subsequent calculations were executed according to Matano procedure. The treatment was applied only to diffusion stages when the condition of infinite sources at periodically disposed boundaries was valid. The results obtained are shown in Table 1 which illustrates shift of the Matano plane followed by the multilayer symmetry factor change at the constant effective interdiffusion coefficient.

The partial diffusion coefficients obtained from these data are 1.98×10^{-20} cm²/s for EuS and 2.6×10^{-22} cm²/s for PbSe.

4. Conclusions

The regular shift of the average peak at Bragg X-ray diffraction on EuS–PbSe multilayer and peculiar behav-

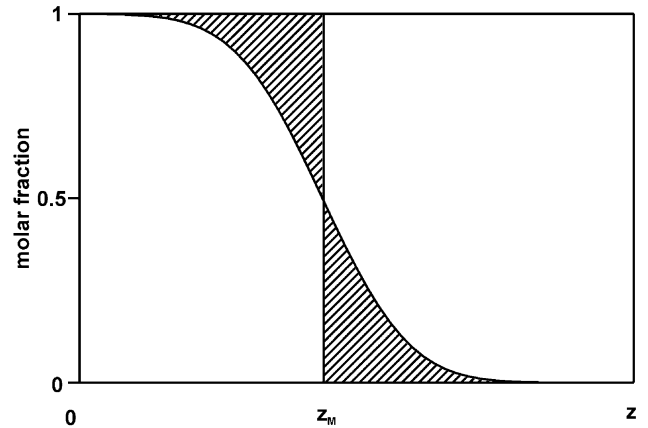


Fig. 5. Definition of the Matano plane position on the concentration profile. Hatched areas corresponds to the integrals in Eq. (6).

Table 1
Calculated characteristics of EuS–PbSe multilayer

Annealing time (min)	z_M (10^{-8} cm)	S	D_{eff} (10^{-21} cm ² /s)
15	7.704	0.144	10.05
30	7.651	0.143	10.04
60	7.597	0.142	10.02
120	7.490	0.140	10.01
180	7.330	0.137	10.03

D_{eff} is effective interdiffusion coefficient.

our of diffraction patterns in the course of diffusion intermixing indicate the change in the layer thickness relation. This means the presence of Kirkendall effect in the specimen. The multilayer profiles restored from the diffraction patterns were treated by Matano process and yielded the values of partial diffusion coefficients of components. It should be stated that obtained effective and partial coefficients are much less than those for PbTe–PbSe multilayer [10]. This may be due to a lesser difference in covalent radii for the last pair of components as compared to PbSe–EuS. The Matano plane in the process of diffusion moves towards the more fusible PbSe component.

Acknowledgments

This work was partly supported by CRDF Award No. UP2-2444-KH-02.

References

- [1] V.N. Lutskii, V.A. Petrov, A.S. Rylik, E.V. Galkina, A.Yu. Sipatov, A.I. Fedorenko, A.G. Fedorov, Phys. Low-Dim. Struct. 7 (1994) 37.

- [2] T.C. Harman, D.L. Spears, M.J. Manfra, *J. Electron. Mater.* 25 (1996) 1121.
- [3] C.F. Majkrzak, T. Story, P. Kacman, R.R. Galazka, K. Ha, H.J.M. de Jonge, A.Yu. Sipatov, V. Volobuev, T.M. Giebultowicz, *Europhys. Lett.* 56 (2001) 54.
- [4] M.A. Hollanders, B.J. Thijsse, E.J. Mittemeijer, *Phys. Rev. B* 42 (1990) 5481.
- [5] W.H. Wang, H.Y. Bai, M. Zhang, J.H. Zhao, X.Y. Zhang, W.K. Wang, *Phys. Rev. B* 59 (1999) 10811.
- [6] J. Burgeat, D. Taupin, *Acta Crystallogr. A* 24 (1968) 99.
- [7] D.L. Windt, *Comput. Phys.* 12 (1998) 360.
- [8] A.V. Vinogradov, I.V. Kozhevnikov, in: A.N. Orajevsky (Ed.), *X-Ray Optics, Proceedings of P.N. Lebedev Institute*, vol. 196, Nauka, Moscow, 1989, p. 62 [in Russian].
- [9] C. Matano, *Jap. J. Phys.* 8 (1933) 109.
- [10] A.G. Fedorov, I.A. Shneiderman, A.Yu. Sipatov, E.V. Kaidalova, *J. Cryst. Growth* 198/199 (1999) 1211.
- [11] S.I. Velmizov, V.K. Gartman, L.A. Klinkova, *Inorg. Mater.* 19 (1983) 31, in Russian.